# **ORIGINAL RESEARCH ARTICLE**

# Numerical simulation of dielectric barrier discharge in Ar/He and $Ar/O_2$ mixtures at atmospheric pressure

Ismail Benchebiba<sup>1\*</sup>, Mohamed Mostefaoui<sup>1</sup>, Abdelatif Gadoum<sup>1,2,3</sup>, Ahmed Nour El Islam Ayad<sup>2,4</sup>, Djilali Benyoucef<sup>1</sup>

#### **ABSTRACT**

This study presents a numerical investigation of dielectrique barrier discharge (DBD) at atmospheric pressure, focusing on two gas mixture: Ar/He and Ar/O<sub>2</sub>. The objective is to analyse the impact of dielectric permittivity on the plasma behavior in the Ar/He mixture, and the influence of the gas temperature in the Ar/O<sub>2</sub> mixture. For the Ar/He case, the relative permittivity of the dielectric is varied from 2 to 12, considering 7 species and 10 chemical reactions. In the Ar/O<sub>2</sub> case, the gas temperature is increased from 350 K to 600 K, with 9 species and 24 chemical reactions taken into account. Key plasma parameters such as species number densities (both neutral and charged), electron temperature, and electron density are evaluated for each scenario. Simulation results for the Ar/He mixture show that increasing dielectric permittivity does not affect the number densities of Ar, He, He<sup>+</sup>, or Hes, but leads to increased densities of electrons, Ars, Ar<sup>+</sup>, and a rise in electron temperature. For the Ar/O<sub>2</sub> mixture, increasing gas temperature causes a reduction in all species densities, while simultaniously increasing the electron temperature.

Keywords: atmospheric pressure; dielectric barrier discharge; plasma density; permittivity; temperature; gas mixtures

#### ARTICLE INFO

Received: 26 May 2025 Accepted: 4 August 2025 Available online: 26 August 2025

#### **COPYRIGHT**

Copyright © 2025 by author(s). Applied Chemical Engineering is published by Arts and Science Press Pte. Ltd. This work is licensed under the Creative Commons Attribution-NonCommercial 4.0 International License (CC BY 4.0).

https://creative commons.org/licenses/by/4.0/

#### 1. Introduction

Recent years have witnessed growing interest in various plasma generation techniques<sup>[1,5]</sup>. Among these, dielectric barrier discharge (DBD) has emerged as a prominent method due to its unique advantages and its substantial contributions to plasma physics and chemistry<sup>[6–8]</sup>. DBD occurs between two electrodes separated by an insulating layer and facilitates the transition of a neutral gas or gas mixture into a plasma state, where diverse active species such as ions, excited atoms/molecules, and radicals are generated<sup>[9–11]</sup>.

ISSN: 2578-2010 (O)

In addition to experimental work<sup>[12]</sup>, numerical simulations play a critical role in predicting and analyzing the complex dynamics of plasma systems<sup>[13]</sup>. Modeling plasma discharges, especially DBDs, requires a comprehensive understanding of the microscopic processes and chemical reactions involved. These reactions depend on parameters such as electron temperature, gas temperature, and reaction-specific rate coefficients.

Numerical studies offer a valuable framework to assess the influence of various physical and operational parameters on DBD

<sup>&</sup>lt;sup>1</sup> LGEER Laboratory, Faculty of Technology, Hassiba Benbouali University of Chlef, 02000, Algeria

<sup>&</sup>lt;sup>2</sup> Electrical Engineering Department Faculty of Applied Sciences, Kasdi Merbah University of Ouargla, 30000, Algeria

<sup>&</sup>lt;sup>3</sup> LRPPS Laboratory, Faculty of Mathematics and Material Sciences, Kasdi Merbah University of Ouargla, 30000, Algeria

<sup>&</sup>lt;sup>4</sup> APELEC Laboratory, Djilali Liabes University, Sidi Bel Abbes, 22000, Algeria

<sup>\*</sup>Corresponding author: Ismail Benchebiba, i.benchebiba@univ-chlef.dz

performance. For instance, in one-dimensional simulations of DBDs for hydrogen and hydrocarbon production from pure methane, parameters like applied voltage, frequency, gas pressure, and dielectric capacitance were investigated. Considering 17 species and 46 reactions, it was shown that applied voltage and dielectric capacitance are key to optimizing methane conversion and hydrogen yield<sup>[14]</sup>. Another study, involving 20 species and 37 reactions, demonstrated that increasing voltage, pressure, dielectric capacitance, and the secondary electron emission coefficient significantly contributes to gas heating in methane-fed DBDs<sup>[15]</sup>.

Furthermore, DBD studies are not limited to common gases. There is increasing interest in using noble gases or their mixtures with reactive gases as working media. For example, numerical simulations of atmospheric-pressure argon DBDs (considering 6 species and 8 reactions) have shown that increasing gas temperature decreases peak ionization rates, induces a shift from alpha to alpha-gamma discharge modes, and highlights the relevance of ground-state ionization, excitation, and three-body quenching processes<sup>[16]</sup>.

The paper is organized as follows: Section 2 outlines the discharge model and simulation approach. Section 3 presents and discusses the simulation results. The concluding section summarizes the findings and contributions of the study. This work aims to enrich the numerical literature on dielectric barrier discharges by offering a comparative analysis of two different gas mixtures—an area still underrepresented in current research.

#### 2. Materials and Methods

## 2.1. Schematic of dielectric barrier discharge

**Figure 1** shows the schematic of the barrier discharge reactor modelled in this study. It consists of: two electrodes, one of which is connected to a sinusoidal voltage and the other to ground, a discharge gap between two insulating layers. The insulating layer covered by the high-voltage electrode is called the high-voltage dielectric, and the insulating layer connected to the ground electrode is called the grounded dielectric.

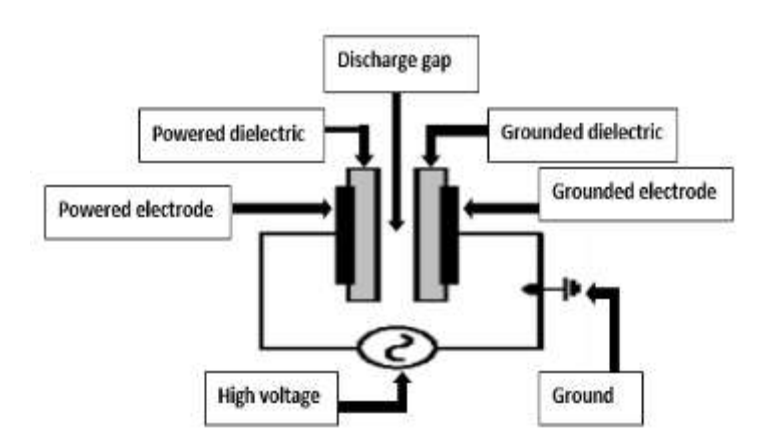


Figure 1. Schematic of dielectric barrier discharge.

The 1D model of the dielectric barrier discharge reactor is shown in **Figure 2**. Where 1 is the outer boundary of the powered electrode to which the sinusoidal voltage is applied, 2 is the inner boundary of the powered electrode, 3 is the internal boundary of the grounded electrode, 4 is the outer boundary of the grounded electrode, 5 is the distance between the powered electrode boundaries of 0.1 mm, 6 is the discharge gap distance between the inner powered electrode boundary and inner grounded electrode boundary of 0.1 mm, 7 is the distance between the grounded electrode boundaries of 0.1 mm. The 1D model has the advantage of shorter computation time compared to the 2D model<sup>[18,19]</sup>, in addition to the possibility of accessing important information about the properties of the plasma, including the densities of species. However, information about

the fluxes of species towards the electrodes as a function of radial distance remains inaccessible, which is one of the most significant drawbacks of the 1D model, as pointed out in<sup>[20]</sup>.

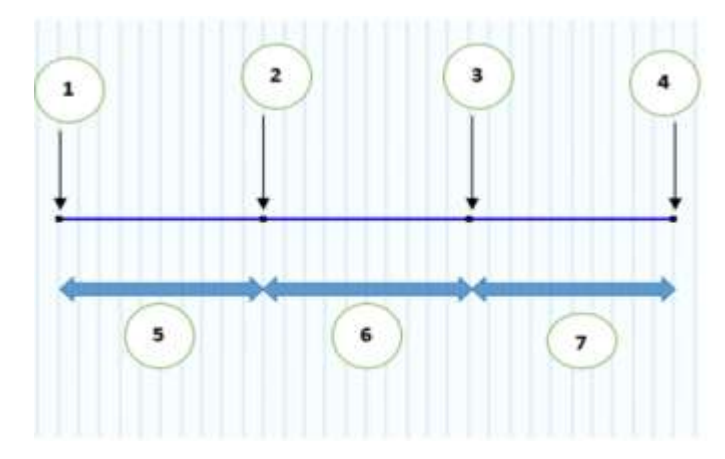


Figure 2. 1D model of dielectric barrier discharge.

#### 2.2. Chemical reactions for Ar/He and Ar/O2 mixtures

The chemical reactions that occur during the discharge phenomena in the Ar/He and Ar/O<sub>2</sub> mixtures are listed in **Table 1** and **Table 2**, respectively. The rate coefficients of the reactions, for which cross section data are used, are denoted as  $f_M(CS)$  and are calculated by a convolution of the cross section with a Maxwellian electron velocity distribution function. T is the gas temperature and  $T_e$  is the electron temperature with units of K and eV, respectively. The number of species are 7 and 9, and the number of chemical reactions are 10 and 24 for Ar/He and Ar/O<sub>2</sub> mixtures, respectively. Some chemical species are not considered in both gas mixtures, such as: He<sub>2</sub> , He<sub>2</sub><sup>+</sup> , Ar<sub>2</sub>, Ar<sub>2</sub><sup>+</sup>, O<sub>3</sub> , O<sub>2</sub>(a $\Delta_g$ ) and O<sub>2</sub><sup>-</sup>, in addition to the absence of some other possible chemical reactions and collisions pathways such as: metastable pooling (Hes + Hes), penning ionization (Hes + Ar) and ozone production (O + O<sub>2</sub> + O<sub>2</sub>  $\rightarrow$  O<sub>3</sub> + O<sub>2</sub>). Although some particles and chemical reactions may play an important role in plasma chemistry, they are sometimes deliberately ignored due to their limited impact on the desired results, even when they occur in reality. This makes the poverty of chemical reactions data a theoretical necessity in some simulation cases.

Table 1. List of chemical reactions for Ar/He mixture model.

Reactions	Rate coefficients	Reference
$e + He \rightarrow e + He$	f <sub>M</sub> (CS)	[21,22]
$e + He \rightarrow e + Hes$	$f_M(CS)$	[21,22]
$e + He \rightarrow e + e + He^+$	f <sub>M</sub> (CS)	[21,22]
$e + Ar \rightarrow e + Ar$	$f_M(CS)$	[23]
$e + Ar \rightarrow e + Ars$	$f_M(CS)$	[23]
$e + Ars \rightarrow e + Ar$	f <sub>M</sub> (CS)	[23]
$e + Ar \rightarrow e + e + Ar^+$	$f_M(CS)$	[23]
$e + Ars \rightarrow e + e + Ar^+$	$f_M(CS)$	[23]
$Ars + Ars \rightarrow e + Ar + Ar^{+}$	$6.2 \times 10^{-10} \text{ m}^3 \text{s}^{-1}$	[24,25]
$Ars + Ar \rightarrow Ar + Ar$	$3\times10^{-15} \text{ m}^3\text{s}^{-1}$	[24,25]

Table 2. List of chemical reaction for Ar/O<sub>2</sub> mixture model.

Reactions	Rate coefficients	References
$Ar + e \rightarrow e + Ar$	f <sub>M</sub> (CS)	[23]
$Ar + e \rightarrow e + Ars$	$f_M(CS)$	[23]
$Ars + e \rightarrow e + Ar$	$f_M(CS)$	[23]
$Ar + e \rightarrow Ar^+ + e + e$	$f_{M}(CS)$	[23]
$Ars + e \rightarrow Ar^+ + e + e$	$f_M(CS)$	[23]
$Ars + Ars \rightarrow Ar + Ar^{+} + e$	$6.2 \times 10^{-16} \text{ m}^3 \text{s}^{-1}$	[24,25]
$Ars + Ar \rightarrow Ar + Ar$	$3\times10^{-21}$ m <sup>3</sup> s <sup>-1</sup>	[24,25]
$Ar^+ + e + e \rightarrow Ar + e$	$8.75 \times 10^{-39} T_e^{-4.5} m^3 s^{-1}$	[26]
$O_2 + e \rightarrow O_2 + e$	$4.7 \times 10^{-14} T_e^{-0.5} m^3 s^{-1}$	[26]
$O_2 + e \rightarrow O + O + e$	$6.86 \times 10^{-15} exp(-6.29/T_e) m^3 s^{-1}$	[27]
$O^- + e \rightarrow O + e + e$	$5.47 \times 10^{-14}  T_e^{0.324}  exp(-2.98/T_e)  m^3 s^{-1}$	[28]
$O + e \rightarrow O^+ + e + e$	$9 \times 10^{-15} \mathrm{T_e^{0.7}\ exp(-13.6/T_e)}\ m^3 s^{-1}$	[28]
$O_2 + e \rightarrow O_2^+ + e + e$	$2.34 \times 10^{-15}  T_e^{1.03}  exp(-12.29/T_e)  m^3 s^{-1}$	[28]
$O_2 + e \rightarrow O + O^-$	$1.07 \times 10^{-15}  \text{Te}^{-1.391}  \exp(-6.26/\text{Te})  \text{m}^3 \text{s}^{-1}$	[28]
$O_2 + e \rightarrow O^+ + O + e + e$	$1.88 \times 10^{-16}  \text{T}_e^{1.699}  \text{exp}(-16.81/T_e)  \text{m}^3 \text{s}^{-1}$	[28]
$\mathrm{O}^+ + \mathrm{O}_2 \rightarrow \mathrm{O} + \mathrm{O}_2^+$	$2 \times 10^{-17} (300/T)^{0.5} \text{ m}^3 \text{s}^{-1}$	[26]
$O + O_+ \longrightarrow O + O$	$4\times10^{-14}(300/T)^{0.44} \text{ m}^3\text{s}^{-1}$	[28]
$O^- + O_2^+ \rightarrow O + O + O$	$2.6 \times 10^{-14} (300/T)^{0.44} \text{ m}^3 \text{s}^{-1}$	[28]
$O^- + O_2^+ \rightarrow O + O_2$	$2.6 \times 10^{-14} (300/T)^{0.44} \text{ m}^3 \text{s}^{-1}$	[28]
$O^- + O \rightarrow O_2 + e$	$3\times10^{-16} \text{ m}^3\text{s}^{-1}$	[26]
$O + O + O_2 \rightarrow O_2 + O_2$	$3.81\times10^{-42}$ exp(-177/T)/T m <sup>6</sup> s <sup>-1</sup>	[29]
$O^- + Ar^+ \rightarrow O + Ar$	$4 \times 10^{-14} (300/T)^{0.43} \text{ m}^3 \text{s}^{-1}$	[30]
$Ar + O_2^+ \rightarrow O_2 + Ar^+$	$2.1 \times 10^{-17} \text{ m}^3 \text{s}^{-1}$	[30]
$Ar^+ + O_2 \rightarrow O_2^+ + Ar$	$4.9 \times 10^{-17} (300/T)^{0.78} + \exp(-5027.6/T) \text{ m}^3 \text{s}^{-1}$	[31]

## 2.3. Model equations

The drift-diffusion equation<sup>[32]</sup> for electron density and mean electron energy are given by Eq.(1), where  $n_e$  is the electron density,  $\mu_e$  is the electron mobility,  $D_e$  is the electron diffusivity and  $R_e$  is the electron source term.

$$\frac{\partial n_e}{\partial t} + \nabla [-n_e(\mu_e E) - D_e \nabla n_e] = R_e$$
 (1)

The electron diffusivity  $D_e$ , the energy mobility  $\mu_e$  and the energy diffusivity  $D_e$  are given by Eq.(2), Eq.(3) and Eq.(4), respectively:

$$D_e = \mu_e T_e \tag{2}$$

$$\mu_{\epsilon} = \frac{5}{3}\mu_{e} \tag{3}$$

$$D_{\epsilon} = \mu_{\epsilon} T_{e} \tag{4}$$

The electron source term is given by Eq.(5), where  $x_j$  is the mole fraction of the target species for reaction j,  $k_j$  is the rate coefficient for reaction j, and  $N_n$  is the total neutral number density.

:

$$R_e = \sum_{j=1}^{M} x_j k_j N_n n_e \tag{5}$$

The electron energy loss is obtained by summing the collision energy loss over all reactions as given by Eq.(6), where  $\Delta \epsilon_i$  is the energy loss of reaction.

$$R_{\varepsilon} = \sum_{j=1}^{P} x_j k_j N_n n_e \Delta \epsilon_j \tag{6}$$

For the dielectrics, the electric field, the electric displacement, and charge conservation laws are given by Eq.(7), Eq.(8), and Eq.(9) respectively:

$$E = -\nabla V \tag{7}$$

$$D = \varepsilon_0 \varepsilon_r E \tag{8}$$

$$\nabla \cdot \mathbf{D} = \mathbf{\rho} \tag{9}$$

Where E is the electric field, D is the electric displacement,  $\epsilon_0$  and  $\epsilon_r$  are the vacuum permittivity and dielectric relative permittivity, respectively, and  $\rho$  is the surface charge density.

The boundary conditions for the electron flux and electron energy are given by Eq.(10) and Eq.(11), respectively, where  $v_{e,th}$  is the threshold electron energy and  $\gamma_i$  is the secondary electron emission coefficient.

$$\mathbf{n} \cdot \Gamma_{\mathbf{e}} = \left(\frac{1}{2} \mathbf{v}_{\mathbf{e}, \mathsf{th}} \mathbf{n}_{\mathbf{e}}\right) - \left(\sum \gamma_{j} \left(\Gamma_{j} \cdot \mathbf{n}\right)\right) \tag{10}$$

$$n \cdot \Gamma_{\epsilon} = \left(\frac{5}{6} v_{e,th} n_{\epsilon}\right) - \left(\sum \gamma_{j} \, \epsilon_{j} \left(\Gamma_{j} \cdot n\right)\right) \tag{11}$$

At the outer grounded electrode boundary, the electrical potential must be zero according to Eq.(12):

$$V = 0 \tag{12}$$

At the outer high-voltage electrode boundary the applied voltage is given by Eq.(13), where  $V_{max}$  is the amplitude of the applied voltage and f is the frequency:

$$V = -V_{\text{max}}\sin(2\pi ft) \tag{13}$$

#### 3. Results and Discussion

#### 3.1. Results of Ar/He mixture model: The role of dielectric relative permittivity

The behavior of Ar/He plasma mixture is analyzed under a 1 kV peak sinusoidal voltage at 13.56 MHz frequency, at a gas temperature of 400 K and atmospheric pressure. The initial values of the electron, He<sup>+</sup> and Ar<sup>+</sup> densities are taken as  $2 \times 10^{13}$  m<sup>-3</sup>,  $1 \times 10^{13}$  m<sup>-3</sup> and  $1 \times 10^{13}$  m<sup>-3</sup> respectively.

The influence of dielectric relative permittivity  $\varepsilon_r$  on the electric field distribution is shown in **Figure 3(a)** for  $\varepsilon_r$  =2 and **Figure 3(b)** for  $\varepsilon_r$  =12. In both cases, the spatiotemporal electric field shows double-peaked structure with a positive peak near the right boundary and negative peak near the left boundary due to the alternating nature of the applied RF voltage. These peaks reflect the local enhancement of the sheath fields during different half-cycles of the RF waveform.

Interestingly, the peak values of the electric field are strongly affected by  $\varepsilon_r$ . For  $\varepsilon_r$  =2, the positive electric field peak reaches 12.2kV/mm, while the peak is much higher 41.8 kV/mm for  $\varepsilon_r$  =12. This is consistent with the dielectric effect on voltage drop: higher permittivity concentrates more of the voltage across the plasma

bulk, increasing the field strength inside it. Although the spatial spread of the field is more pronounced for  $\varepsilon_r$  =2, the magnitude is significantly higher for  $\varepsilon_r$ =12, leading to enhanced energy transfer to electrons.

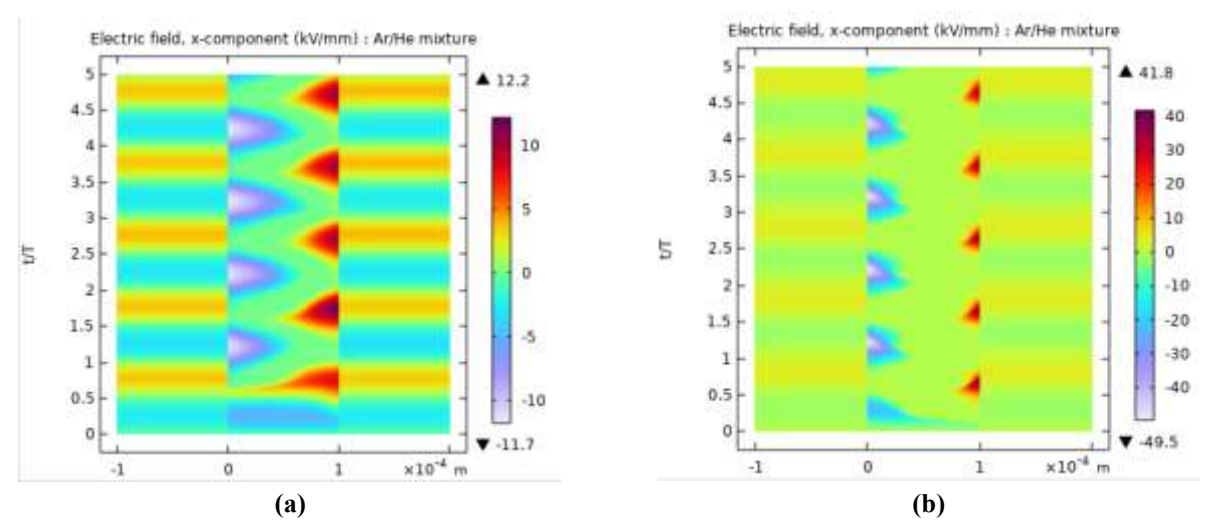


Figure 3. Spatiotemporal distribution of electric field strength for : (a)  $\varepsilon_r = 2$ ; (b)  $\varepsilon_r = 12$ .

Since the electron temperature is directly linked to the local electric field through the energy gained from the RF oscillations, the increased electric field at  $\varepsilon_r$  =12 results in a higher electron temperature. The data in **Figure 4(a)** confirm this, showing an increase in the electron temperature from 7.2 eV for  $\varepsilon_r$  =2 to 19.1 eV for  $\varepsilon_r$  =12. As a consequence, the more energetic electrons enhance ionization rates, increasing the electron density from  $1.84 \times 10^{19}$  to  $1.96 \times 10^{20}$  m<sup>-3</sup>, as shown in **Figure 4(b)** this underlines the strong impact of dielectric permittivity on the power deposition into the plasma via the modulation of the internal electric field.

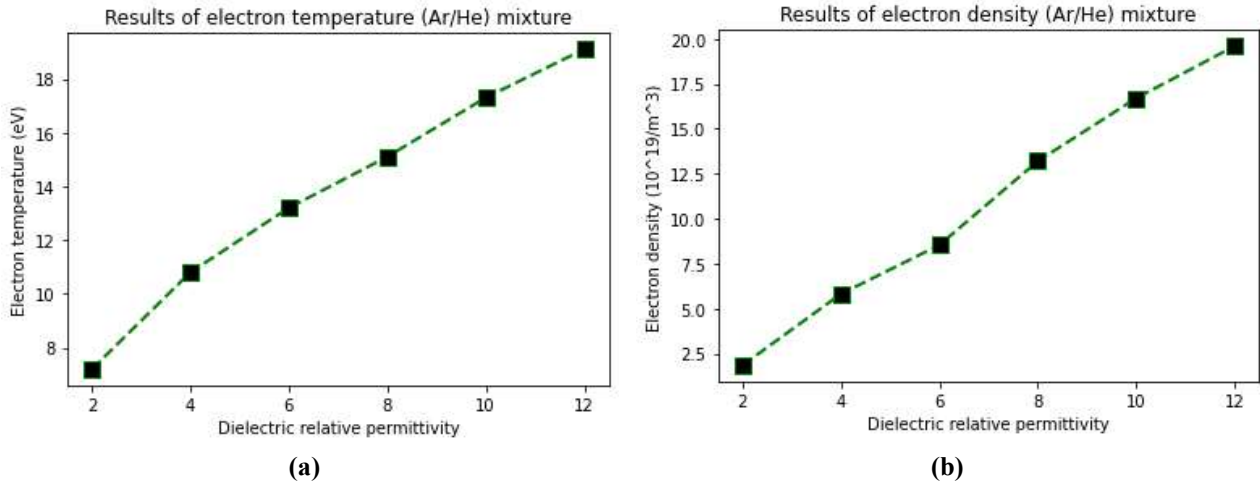


Figure 4. The effect of dielectric permittivity on Ar/He mixture characteristics: (a) Electron temperature; (b) Electron number. Density.

While  $\varepsilon_r$  has a clear influence on the plasma's charged particle behavior, it does not affect the neutral gas densities, since it does not alter the gas temperature. The densities of Argon and Helium gases remain constant, governed solely by the fixed operating temperature and pressure. As shown in **Figure (5a)**, the argon gas density remain  $1.83 \times 10^{25}$  m<sup>-3</sup>, which is orders of magnitude higher than the electron density. This abundance of neutral Ar atoms provides a rich reservoir for electron impact reactions, particularly ionization and excitation.

Due to the increased electron density and energy at higher  $\varepsilon_r$ , the production of  $Ar^+$  and excited argon Ars increases. This is evident in **Figure (6a)** and **Figure (7a)**, where  $Ar^+$  density rises from  $2.85 \times 10^{19}$  to  $2.33 \times 10^{20}$ 

 $m^{-3}$ , and the excited species Ars increases from  $1.54 \times 10^{20}$  to  $1.37 \times 10^{21}$  m<sup>-3</sup>. These changes confirm that the energy gain by electrons due to stronger fields significantly enhances the overall argon plasma chemistry.

On the other hand, helium behaves differently do to its low neutral gas density, which remains at  $3.65 \times 10^{17}$  m<sup>-3</sup>, as shown in **Figure (5b)**. This density is much lower than the electron density, meaning that helium species are not dominant player in the plasma chemistry under the given conditions. As a result the densities of He<sup>+</sup> and excited helium Hes show negligible variation with  $\epsilon_r$ , maintaining values around  $1.12 \times 10^{13}$  m<sup>-3</sup> and  $1.83 \times 10^{17}$  m<sup>-3</sup> respectively, as seen in **Figures (6b)** and **(7b)**. This indicates that although the electric field and electron temperature increase, the scarcity of helium atoms prevents significant changes in their associated reaction rates.

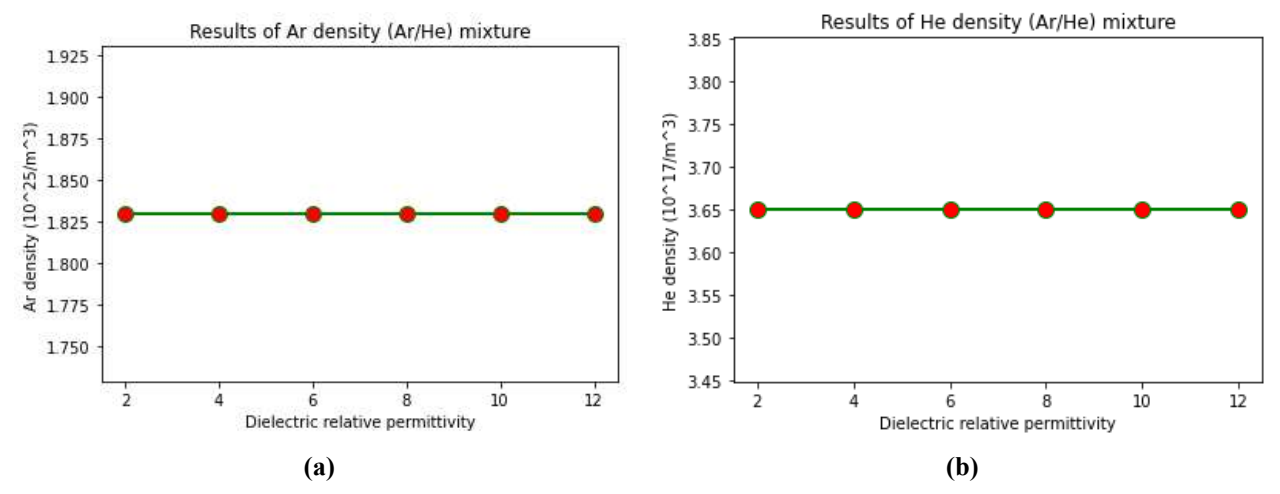


Figure 5. The effect of dielectric permittivity on Ar/He mixture characteristics: (a) Ar number density; (b) He number density.

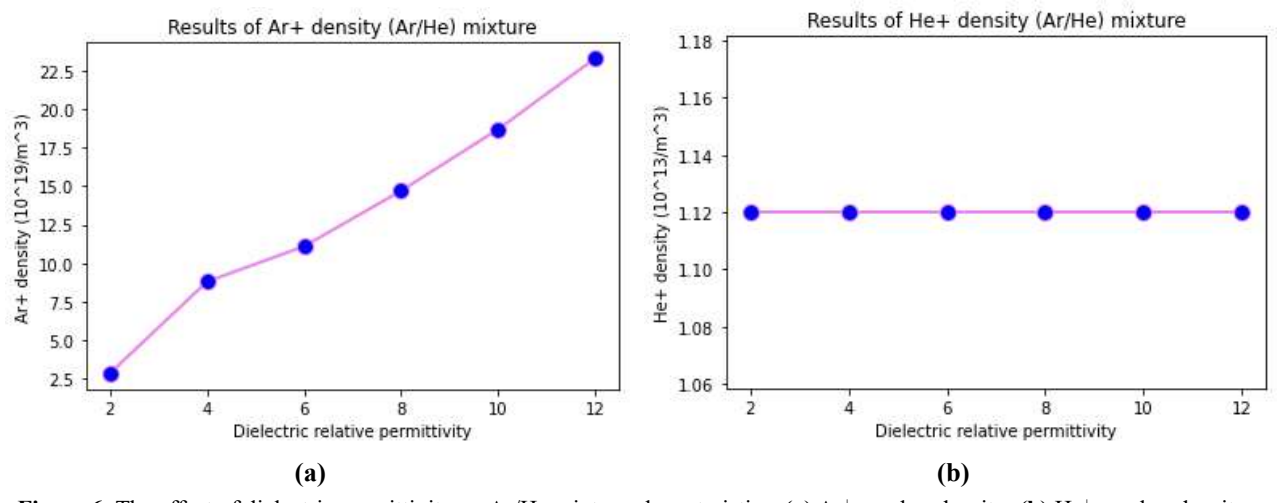


Figure 6. The effect of dielectric permittivity on Ar/He mixture characteristics: (a) Ar<sup>+</sup> number density; (b) He<sup>+</sup> number density.

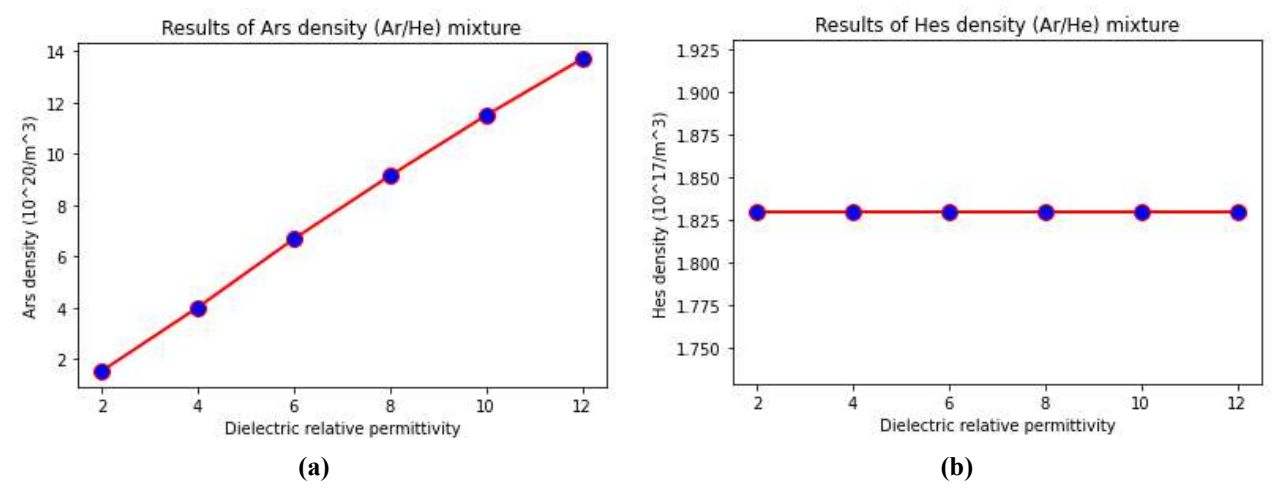


Figure 7. The effect of dielectric permittivity on Ar/He mixture characteristics: (a) Ars number density; (b) Hes number density.

In conclusion, the dielectric relative permittivity significantly alters the internal electric field distribution, which in turn affects the energy and density of electrons. These changes drive ionization and excitation processes, particularly for argon due to its high neutral density. However species like helium, which are present in much lower quantities, do not respond strongly to the same field changes. This analyses highlights the importance of considering both plasma energy dynamics and neutral species availability in understanding the effects of dielectric properties on plasma behavior. This can be seen in the experimental work of  $^{[33]}$ , where Norberg, S. A et al, evaluated how different dielectric substrates with permittivity in range 2–80 affect electric fields, ionization waves, and electron temperatures in atmospheric-pressure argon plasmas. It showed that higher  $\epsilon_r$  increases electric field strength and ionization wave speed mirroring your observations relating  $\epsilon_r$  to electron heating.

#### 3.2. Results of Ar/O<sub>2</sub> mixture model: The role of gas temperature

The influence of gas temperature on the plasma behavior in an Ar/O<sub>2</sub> mixture is investigated under 700 V peak sinusoidal voltage at 13.56 MHz, with a dielectric relative permittivity of 10, at atmospheric pressure. The initial particle densities-electrons, Ar<sup>+</sup>, O<sub>2</sub><sup>+</sup>, O<sup>+</sup>, and O<sup>-</sup> are  $20 \times 10^{10}$  m<sup>-3</sup>,  $10 \times 10^{10}$  m<sup>-3</sup>,  $10 \times 10^{10}$  m<sup>-3</sup>,  $10 \times 10^{10}$  m<sup>-3</sup>, respectively.

At constant atmospheric pressure; increasing the gas temperature reduces the total number density of neutral particles, as described by the relation  $n_n = 7.3416 \times 10^{21} / T_g$  [16], where  $n_n$  and  $T_g$  are the gas density and gas temperature, respectively. This leads to a clear reduction in both argon and oxygen neutral gas densities.

As shown in **Figure 7(a)**, the argon density decreases from  $21 \times 10^{24}$  to  $12.2 \times 10^{24}$  m<sup>-3</sup>, while **Figure 7(b)**. shows the oxygen density decreases from  $32.1 \times 10^{16}$  to  $18.6 \times 10^{16}$  m<sup>-3</sup>. This decline in neutral species impacts the frequency of electron-neutral collisions, reducing the number of inelastic interactions in the plasma.

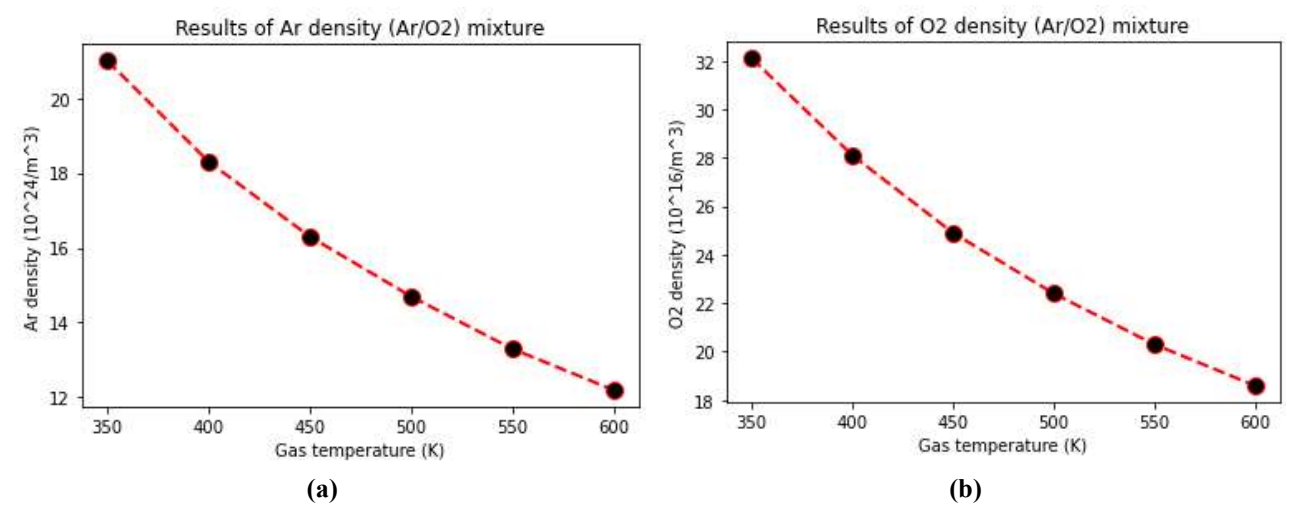


Figure 8. The effect of gas temperature on Ar/O<sub>2</sub> mixture characteristics: (a) Ar number density; (b) O<sub>2</sub> number density.

The reduced collisions rate means that electrons lose less energy in each cycle of the RF field, causing an increase in their average energy. This is illustrated in **Figure 8(a)**, where the electron temperature rises from 13.3 eV to 19.2 eV as the gas temperature increases. However, the elevated electron energy does not lead to a higher electron density. On the contrary, as shown in **Figure 8(b)**, the electron density decreases from  $16.1 \times 10^{19}$  to  $13.5 \times 10^{19}$  m<sup>-3</sup>. This seemingly paradoxical result can be explained by the strong dependence of ionization rates not only on electron energy, but also on the availability of neutral gas targets. While energetic electrons are more capable of inducing ionization, the lack of neutral atoms limits the overall rate of electron production.

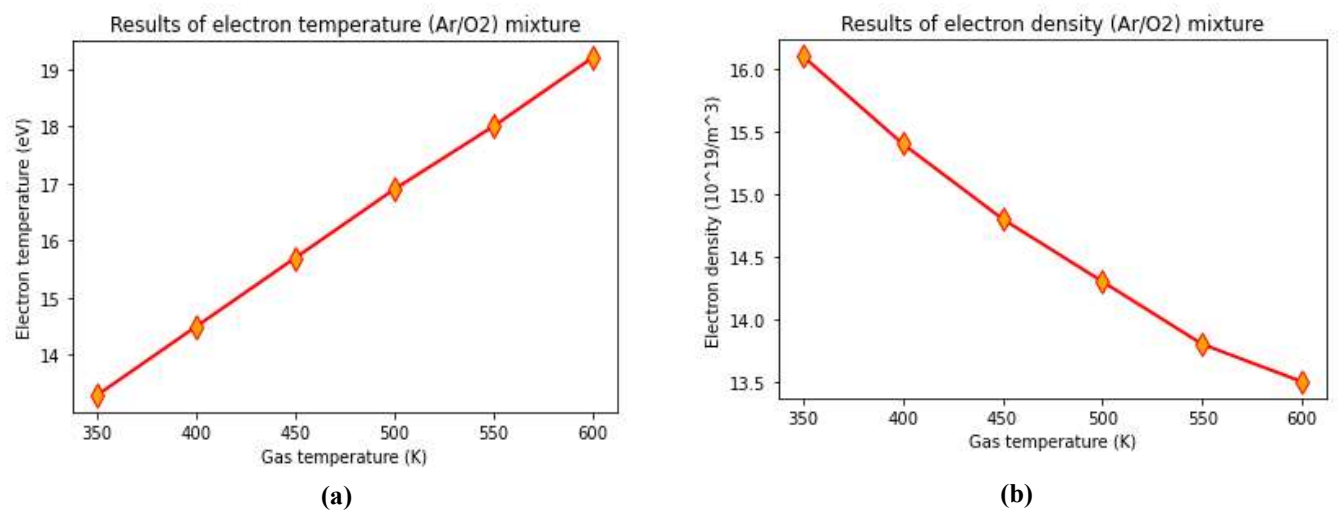


Figure 9. The effect of gas temperature on Ar/O<sub>2</sub> mixture characteristics: (a) Electron temperature; (b) Electron number density.

For argon-related reactions; this phenomenon is clearly observed. The ionization of argon (e + Ar  $\rightarrow$  e + e + Ar<sup>+</sup>) and the excitation process (e + Ar  $\rightarrow$  e + Ars) both depend heavily on the density of neutral argon atoms. As the argon density decreases, the rates of these reactions also decline. As a result, **Figure 9(b)** shows the Ar<sup>+</sup> ion density decreasing from  $31.5 \times 10^{19}$  to  $23.7 \times 10^{19}$  m<sup>-3</sup>, while **Figure 10(a)** reveals a decrease in the excited argon species Ars from  $11.7 \times 10^{20}$  to  $8.88 \times 10^{20}$  m<sup>-3</sup>. These trends confirm that the reduction in neutral gas density suppresses argon plasma chemistry, despite increased electron temperatures.

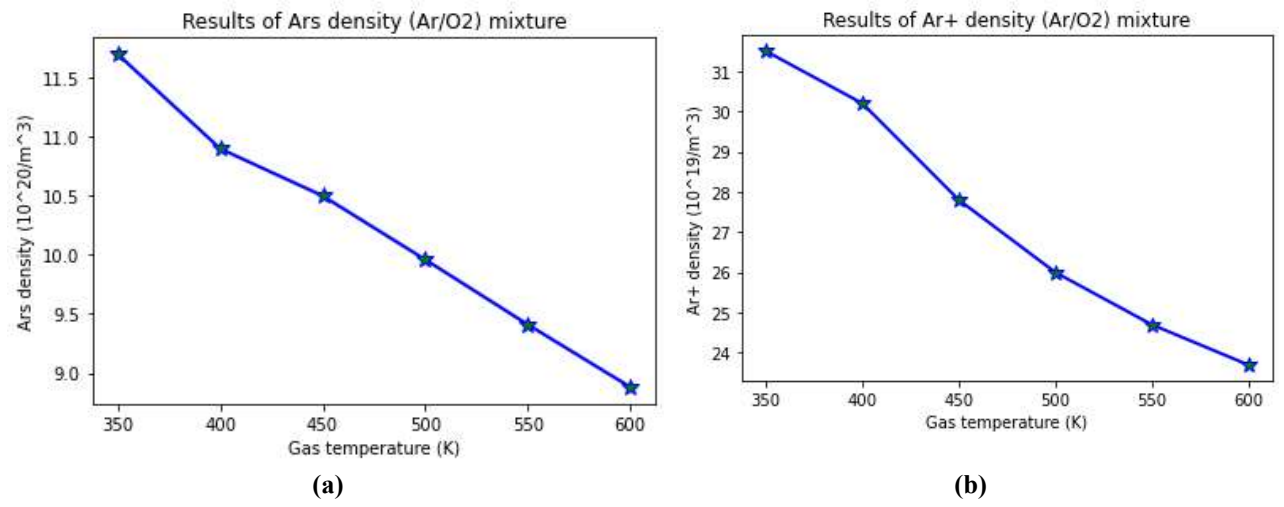


Figure 10. The effect of gas temperature on Ar/O<sub>2</sub> mixture characteristics: (a) Ars number density; (b) Ar<sup>+</sup> number density.

Oxygen-related reactions are similarly affected. The ionization of molecular oxygen ( $O_2 + e \rightarrow O_2^+ + e + e$ ) leads to a decrease in  $O_2^+$  ion density from  $32.6 \times 10^{11}$  to  $18.1 \times 10^{11}$  m<sup>-3</sup>, as shown in **Figure 10(a)**. The dissociative ionization process ( $O_2 + e \rightarrow O^+ + O + e + e$ ) is also limited, with **Figure 10(b)** showing a drop in  $O^+$  density from  $46.2 \times 10^{11}$  to  $34.1 \times 10^{11}$  m<sup>-3</sup>. The reduced  $O_2$  density weakens the formation of atomic oxygen through the dissociation process ( $O_2 + e \rightarrow O + O + e$ ), and as seen in **Figure 11(a)** the O atom density falls from  $21 \times 10^{16}$  to  $12.3 \times 10^{16}$  m<sup>-3</sup>. Moreover, the dissociative attachment reaction ( $O_2 + e \rightarrow O + O^-$ ) becomes less significant, leading to a reduction in  $O^-$  ion density from  $49.3 \times 10^{16}$  to  $32.3 \times 10^{12}$  m<sup>-3</sup>, as shown in **Figure 12(b)**.

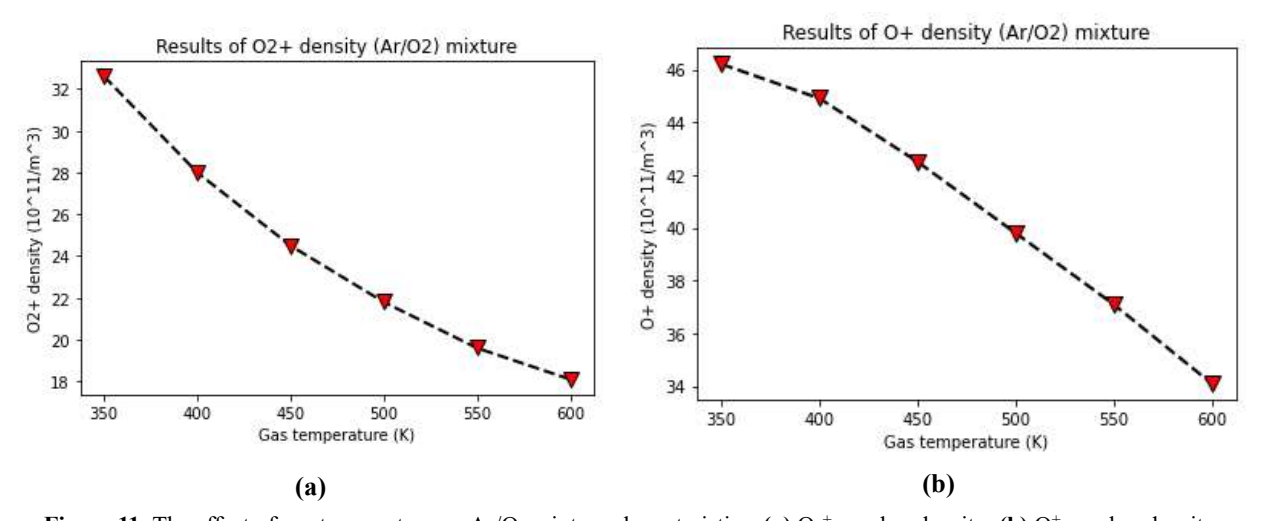


Figure 11. The effect of gas temperature on Ar/O<sub>2</sub> mixture characteristics: (a) O<sub>2</sub><sup>+</sup> number density; (b) O<sup>+</sup> number density.

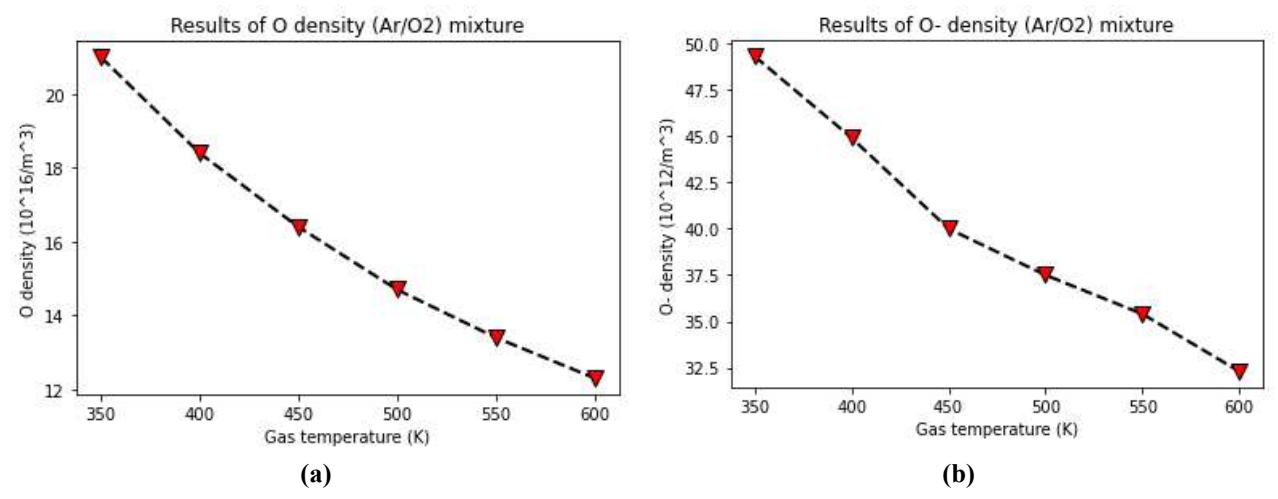


Figure 12. The effect of gas temperature on Ar/O<sub>2</sub> mixture characteristics: (a) O number density; (b) O<sup>-</sup> number density.

Overall, these results illustrate that gas temperature significantly influences the plasma characteristics through its control over neutral particle density. Although higher gas temperatures increase the energy of electrons, they simultaneously reduce the number of collision partners. Consequently, the formation rates of charged and excited species decline. This highlights the complex interplay between energy input and gas phase composition in determining plasma behavior, and underscores the importance of neutral density as a controlling parameter in high frequency atmospheric pressure discharges. The study of Zhang et al<sup>[16]</sup>, using fluid simulations analyzed how neutral gas temperature alters plasma properties in argon DBD at atmospheric pressure. This aligns closely with our findings on how gas temperature reduces neutral density and affects electron behavior.

#### 4. Conclusion

The comparative study of Ar/He and Ar/O<sub>2</sub> plasma mixture highlights the distinct yet complementary roles of dielectric relative permittivity and gas temperature in shaping plasma characteristics under RF excitation at atmospheric pressure. In the Ar/He mixture, increasing the dielectric constant significantly modifies the internal electric field distribution, thereby enhancing electron heating and promoting ionization and excitation particularly for Argon, which is present in high neutral density. Helium, due to its much lower density, contributes minimally to plasma chemistry under these conditions.

In contrast, the Ar/O<sub>2</sub> mixture reveals how increasing the gas temperature reduces the neutral particle density, which in turn limits electron-neutral collisions despite a rise in electron temperature. This results in lower ionization and dissociation rates for both argon and oxygen; underscoring the dominant role of target availability in sustaining plasma reactions.

Together these results emphasis the important of carefully controlling both dielectric properties and gas thermodynamic conditions to optimize plasma performance. A strong electric field may increase electron energy; but without sufficient neutral reactants, the plasma cannot sustain high levels of charged or excited species. This interdependence between energy transfer and species availability must be considered in the design and control of RF-driven plasma, especially for applications in atmospheric pressure environments.

## **Conflict of interest**

The authors declare no conflict of interest.

## References

- 1. Johnson, M. J., Brown, G. H., Boris D. R., Petrova T. B., Walton, S. G. "Two Atmospheric Pressure Plasma Jets Driven by Phase-Shifted Voltages: A Method to Control Plasma Properties at the Plasma–Surface Interface," IEEE Transactions on Plasma Science, 2022, 50(9), pp.2961-2971. https://doi.org/10.1109/TPS.2022.3198826
- Levko D. "Runaway Electrons in Gas Discharges: Insights from the Numerical Modeling". Plasma,2025 8(1),pp12. https://doi.org/10.3390/plasma8010012
- 3. Alexiou S. "Effects of Spiralling Trajectories on White Dwarf Spectra: Remarks on Different Calculations". Plasma.2025, 8(1),pp2. https://doi.org/10.3390/plasma8010002.
- 4. Vassallo E, Saleh M, Pedroni M, Cremona A, Ripamonti D. "Characterization of Tungsten Sputtering Processes in a Capacitively Coupled Argon Plasma". Plasma, 2025, 8(1), pp8. https://doi.org/10.3390/plasma8010008
- 5. Fujera J, Hoffer P, Prukner V, Šimek M. "Quantifying Plasma Dose for Barley Seed Treatment by Volume Dielectric Barrier Discharges in Atmospheric-Pressure Synthetic Air". Plasma,2025, 8(1),pp11 https://doi.org/10.3390/plasma8010011.
- 6. Shvydyuk, K.O., Rodrigues, F.F., Nunes-Pereira, J., Páscoa J.C., Silva, A. P. "Thermal Characterization of Ceramic Composites for Optimized Surface Dielectric Barrier Discharge Plasma Actuators". Actuators, 2025,14(3),pp.127. https://doi.org/10.3390/act14030127.
- 7. Xiao, Y., Tian, Y., Zhan, Y., Zhu, J. "Optimization of a Low-Cost Corona Dielectric-Barrier Discharge Plasma Wastewater Treatment System through Central Composite Design/Response Surface Methodology with Mechanistic and Efficiency Analysis" Sustainability, 2024, 16(2),pp.605. https://doi.org/10.3390/su16020605.
- 8. Korzec, D., Freund, F., Bäuml, C., Penzkofer, P., Beier, O., Pfuch, A., Vogelsang, K., Froehlich, F., Nettesheim, S. Hybrid Dielectric Barrier Discharge Reactor: Production of Reactive Oxygen–Nitrogen Species in Humid Air. Plasma. 2025, 8(3),pp27. https://doi.org/10.3390/plasma8030027
- 9. Liu P, Song Y, Zhang Z. "A Novel Dielectric Barrier Discharge (DBD) Reactor with Streamer and Glow Corona Discharge for Improved Ozone Generation at Atmospheric Pressure". Micromachines. 2021; 12(11):1287. https://doi.org/10.3390/mi12111287
- 10. Wang, X., Liu Y, Tan, Z, Chang, L. "Effects of Oxygen Concentration on the Reactive Oxygen Species Density Under Different Operating Conditions in Atmospheric-Pressure Helium/Oxygen Pulsed Dielectric Barrier Discharge," IEEE Access,7,pp.69748-69757,2019. https://doi.org/10.1109/ACCESS.2019.2919098
- 11. Scaltriti, S. G. Cristofolini, A, Neretti G, "Design and characterization of an Atmospheric Pressure Dielectric Barrier Discharge Reactor for Potential Air Disinfection Applications.," in IEEEAccess,13,pp.45037-45047,2025. https://doi.org/10.1109/ACCESS.2025.3548933
- 12. Nassour, K. et al, "Comparative experimental analysis of ozone generation between surface and volume DBD generators," IEEE Transactions on Dielectrics and Electrical Insulation, 25(2), pp. 428-434, 2018. https://doi.org/10.1109/TDEI.2017.006600
- 13. Saidi, S, Loukil H, Khodja, K. Belasri, A. Caillier B, Guillot, P. "Experimental and Theoretical Investigations of Dielectric Barrier Discharge (DBD) Lamp in Ne/Xe Mixture," IEEE Transactions on PlasmaScience ,50(7),pp.2147-2155,2022. https://doi.org/10.1109/TPS.2022.3176412
- 14. Khadir, N. Khodja, K, Belasri, A. "Methan conversion using a dielectric barrier discharge reactor at atmospheric pressure for hydrogen production" Plasma Sci. Technol. 19(9), pp.095502 ,2017. http://dx.doi.org/10.1088/2058-6272/aa6d6d
- 15. Benmoussa, A. Belasri, A. Larouci, B. Belkharroubi, F, Belmiloud, N. "Gas temperature effect in methane DBD reactor for hydrogen production" Plasma Medicine, 12(3), pp.41-58, 2022. https://doi.org/10.1615/PlasmaMed.2023047179
- 16. Zhang, Z. H., Zhong, K. X., Liu, Y., Wang, W., Wang, Y. N., Yang, D. Z. "Fluid simulation of atmospheric argon RF dielectric barrier discharges: Role of neutral gas temperature." Physics of Plasmas, 31(5),pp.053515.,2024.https://doi.org/10.1063/5.0202078
- 17. Baeva, M., Stankov, M., Trautvetter, T., Methling, R., Hempel, F., Loffhagen, D., Foest, R. (2021). The effect of oxygen admixture on the properties of microwave generated plasma in Ar–O2: A modelling study. Journal of Physics D: Applied Physics, 54(35), pp.355205,2021. https://doi.org/10.1088/1361-6463/ac08cc
- Bera, K., Farouk, B. and Lee, Y.H., 1999. Simulation of Thin Carbon Film Deposition in a Radio-Frequency Methane Plasma Reactor. Journal of the Electrochemical Society, 146(9), p.3264. http://dx.doi.org/10.1149/1.1392465
- 19. Nienhuis, G.J. and Goedheer, W., 1999. Modelling of a large scale reactor for plasma deposition of silicon. Plasma Sources Science and Technology, 8(2), p.295. http://dx.doi.org/10.1088/0963-0252/8/2/310
- 20. Herrebout, D., Bogaerts, A., Yan, M., Gijbels, R., Goedheer, W. Dekempeneer, E. "One-dimensional fluid model for an rf methane plasma of interest in deposition of diamond-like carbon layers". Journal of Applied Physics, 2001, 90(2), pp. 570-579. http://dx.doi.org/10.1063/1.1378059
- 21. Ran S, Wang J, Lei B, et al. Numerical simulation of coaxial-coplanar dielectric barrier discharge in atmospheric helium. AIP Advances. 2022; 12(5): 055209. https://doi.org/10.1063/5.0089080

- 22. Hagelaar GJM, Pitchford LC. Solving the Boltzmann equation to obtain electron transport coefficients and rate coefficients for fluid models. Plasma sources science and technology. 2005; 14(4): 722. https://doi.org/10.1088/0963-0252/14/4/011
- 23. Yanguas-Gil A, Cotrino J, Alves LL. An update of argon inelastic cross sections for plasma discharges. Journal of Physics D: Applied physics. 2005; 38(10): 1588. https://doi.org/10.1088/0022-3727/38/10/014
- 24. Baeva M, Hemel F, Baierl H, et al. Two-and three-dimensional simulation analysis of microwave excited plasma for deposition applications: operation with argon at atmospheric pressure. Journal of Physics D: Applied Physics. 2018; 51(38): 385202. https://doi.org/10.1088/1361-6463/aad537
- 25. Lymberpoulos DP, Economou DJ. Fluid simulation of glow discharge: Effect of metastable atoms in argon. Journal of Applied Physics 1993; 73(8): 3668-3679. https://doi.org/10.1063/1.352926
- 26. Lieberman, M. A., Lichtenberg, A. J. 2005 Principles of Plasma Discharges and Materials Processing (New York: Wiley)
- 27. Corr C. S., Gomez, S., Graham, W. G."Discharge kinetics of inductively coupled oxygen plasmas: experiment and model" Plasma Sources Sci. Technol. .21(5), pp.055024, 2012. https://doi.org/10.1088/0963-0252/21/5/055024
- 28. Gudmundssonn, J. T., Thorsteinsson, E. G. "Oxygen discharges diluted with argon: dissociation processes" PlasmaSourcesSci.Technol,16(2),pp.399–412,2007. https://doi.org/10.1088/0963-0252/16/2/025
- 29. Eliasson, B., Kogelschatz U. 1986 Brown Boveri Forschungstemtrum Report KLR 86-11 C
- 30. Bogaerts, A. "Effects of oxygen addition to argon glow discharges: a hybrid Monte Carlo-fluid modeling investigation" Spectrochimca. ActaB,64,pp.1266-1279,2009 https://doi.org/10.1088/1361-6463/ac08cc
- 31. Kutasi, K., Guerra, V., Sa, P. A. "Theoretical insight into Ar-O2 surface-wave microwave discharges" J. Phys. D: Appl.Phys.43(17),pp.175201,2010. https://doi.org/10.1088/0022-3727/43/17/175201
- 32. W. Hänsch, The drift diffusion equation and its applications in MOSFET modeling. Springer Science & Business Media, 2012.
- 33. Norberg, S. A., Johnsen, E., Kushner, M. J. "Helium atmospheric pressure plasma jets touching dielectric and metal surfaces". J. Appl. Phys. 118(1), pp.013301, 2015. https://doi.org/10.1063/1.4923345